Computational exploration of sub-nano Zn and Cu species on Cu/ZrO_2: Implications for Methanol synthesis

Aku Lempelto, Minttu Kauppinen, and Karoliina Honkala*

Department of Chemistry, Nanoscience Center, P.O. Box 35, FI-40014, University of Jyväskylä, Finland

E-mail: karoliina.honkala@jyu.fi

Abstract

Ternary $Cu/Zn/ZrO_2$ (CZZ) catalysts prepared recently using atomic layer deposition (ALD) have shown increased performance towards methanol synthesis. In the present computational study, we have investigated the structure, composition, and stability of various zinc and copper containing sub-nano size species on a zirconia support. Density functional theory calculations with minima hopping was used to sample the positioning and geometry of supported $Zn_xCu_yO_z$ structures up to 8 metal atoms in total. ZnO monomeric species were found to be energetically more favourable than small clusters, which could suggest a resistance to initial stage agglomeration. Ab-initio thermodynamics revealed that under typical methanol synthesis conditions the complete reduction of ZnO and mixed ZnO/Cu clusters is unfavourable. The investigated ZnO monomers and clusters are able to provide CO_2 activation sites, with the $Cu/ZnO/ZrO_2$ triple interface offering the best stabilization for the adsorbed CO_2. All in all the findings suggest that small ZnO species generated by ALD could be stabilized by the zirconia component, while contact with copper species at the interface benefits CO_2 activation.

Introduction

Methanol synthesis from carbon dioxide and hydrogen is a promising approach to convert anthropogenic greenhouse gas into valuable fuels and platform chemicals. Direct carbon dioxide conversion to methanol (CTM) is an exothermic reaction

$$CO_2(g) + 3H_2(g) \longrightarrow CH_3OH(g) + H_2O(g) \quad \text{(R1)}$$

that requires active and selective catalysts in order to achieve high enough conversion at relatively mild reaction conditions. Conventionally, methanol is produced from syngas using a ternary $Cu/ZnO/Al_2O_3$ (CZA) catalyst. In general, copper based materials, such as the commercial CZA catalyst, are the most well studied catalysts for methanol synthesis directly

from CO_2, as well as syngas. However, relatively low conversion and methanol selectivity remain an issue for such catalysts.[1–5] Further development of active, selective, and stable CTM catalysts is required to improve the commercial process.

Ternary $Cu/Zn/ZrO_2$ (CZZ) systems have shown great promise as active and selective CTM catalysts. Using zirconia as an alternative support leads to increased performance, especially methanol selectivity, as compared to the commercial CZA catalyst.[2,6,7] The ternary CZZ catalysts have been shown to achieve higher production rates, total conversion, and selectivity in methanol synthesis than the binary Cu/ZnO and Cu/ZrO_2 systems alone.[7–9] One possible reason could be the formation of special active sites, such as those at the three material interface, resulting in a synergistic effect.

However, the reaction mechanism, nature of the active site, and the roles that each component plays in the binary and ternary systems are still under debate. This is mainly due to the complexity of the systems, with many different synergies between the metal and oxide components. Several candidate active sites have been brought forward, such as Cu nanoparticles with ZnO overlayers,[10–12] Cu-ZnO and Cu-ZrO_2 interfacial sites,[2,6,9,13–17] and Cu-Zn surface alloys.[3,15,18,19] In general, copper is proposed to be responsible for hydrogen splitting activity, while the oxide components, especially the interfacial sites, are required for activation of CO_2 and stabilization of active surface intermediates.

The structure and performance of CZZ catalysts is sensitive to both the catalyst composition and the preparation method. Many different catalyst preparation methods have been used previously, such as precipitation,[7,9,20,21] colloidal crystal templating,[9] sol-gel,[22] flame-spray pyrolysis,[23] and atomic layer deposition.[8] The preparation method can affect the total surface area of the catalyst, the dispersion and available surface area of the copper phase, and the number of basic sites. However, the structure of the catalyst is a function of the reaction conditions, and several studies have highlighted the importance of structural changes, including formation of active sites, during exposure to reactant gases.[15,23–26] For example, even if the as prepared catalyst contains the CuZn alloy, it may no longer be present

under reaction conditions due to interaction between the catalyst and the reacting gases.[15,24] Even so, the preparation method used is important for the active state of the catalyst, as it is a precursor for the in situ formed structure. Regardless of whether the most active site for the reaction is the interface of Cu and ZnO, or a CuZn alloy, the preparation methods should facilitate increased contact between Cu and Zn components. Controlled tuning of the interaction between ZnO and ZrO_2 could also be desirable, as the interface between the two oxides has been suggested as an active site for CO_2 adsorption and activation.[9]

Atomic layer deposition (ALD) as a synthesis technique enables precise control over the surface structure of the catalyst.[27,28] Recently, ALD has been demonstrated as a promising preparation method for CZZ catalysts.[8] The best performing ALD synthesised CZZ consists of a ZrO_2 support, with Cu nanoparticles or clusters and a low ($\approx$ 0.15 ML) coverage of ZnO monomers distributed on the surface. The best performance was achieved with the sample where ZnO is deposited after copper rather than before. The results suggest that contact between ZnO and copper, but without Cu covering the ZnO units, is important for the high activity. However, the specific structure of the catalyst and the nature of the active site, especially during and after exposure to the reaction conditions, is unclear. Monomeric species are known to be highly mobile and thermodynamically driven to agglomerate into larger structures such as clusters or islands, and eventually nanoparticles.[29–31] On the other hand, dynamic evolution of highly dispersed ZnO clusters into monomeric Zn species on ZrO_2 have been recently observed with operando XAS of CZZ samples prepared with flame-spray pyrolysis.[23] The results suggest that zirconia can stabilize the monomeric Zn species through a strong interaction (facilitated by the preparation method). The atomically dispersed catalyst exhibited superior activity, which was rationalised by a mechanistic DFT study that found the H_2 dissociation to be more favourable at the atomic Zn sites as compared to Cu or Zr sites. To rationalize the structure-performance relationship of ALD prepared CZZ catalysts, it is essential to have information on the structure, relative stability, and interaction with reactant species of the various surface motifs at different reaction conditions.

Previous computational studies have mainly employed two-component models to elucidate the role of different structural motifs found in CZZ and CZA systems.[3,4,9,13,15,16,18,19] The Zn containing models especially differ in where and how the Zn promoter is incorporated into the catalyst. Zn decorated extended copper surface models have been extensively used to mimic sites on alloyed nanoparticles.[3,15,18,19] In some recent models, the Zn promoter is present as an oxide e.g. as small supported clusters[15,16,32,33] or as periodic nano stripes or ribbons.[18,32,34] Naturally, two component models cannot capture effects that could arise at sites that form when all components are in close contact with one another. Three-component models have emerged recently in order to represent those kinds of active sites.[16,17,23] In our previous study, we employed a zirconia supported Cu nanorod with and without Zn incorporated into the interface between the rod and support.[17] The model served as a representative of two and three component metal support interface sites, and was used to elucidate the role of a dilute interfacial CuZn alloy. Our results showed that especially CO_2 activation was promoted by the Zn component.

Although ALD enables the controlled synthesis of monomeric ZnO promoter species on the catalyst surface, it is unclear whether those small species can resist agglomeration under reaction conditions. Furthermore, are the monomers located on the ZrO_2 support, at the metal-support interface, or do they decorate the Cu nanoparticle? The ALD Zn(acac) precursor has thus far been demonstrated to react with the zirconia support, but no comparable data exists for the copper component, which exists as an oxide prior to the reduction treatment. In the present study, we have compared the stability of ZnO monomers at various locations of the possible catalyst domains. Another debated aspect of the nature of Zn promoter is whether it is oxidised[12,15,24,25,35] or alloyed to Cu.[3,36–38] Even though the ALD prepared catalyst should contain ZnO units, it is possible that under the reducing methanol synthesis conditions the ZnO would be reduced and form dilute surface alloys with Cu as have been suggested previously.[39–42]

In our present work, we have investigated the stability and structure of sub-nanoscale

Zn and Cu species on zirconia and copper-based supports by means of density functional theory (DFT), minima hopping global optimization, and ab-initio thermodynamics. We model as-prepared monomeric ALD CZZ structures, as well as possible structures that result from initial stages agglomeration of the Zn monomers on the surface, surface migration, nano-alloying of Cu and Zn, vacancies on the zirconia surface, and oxidation/reduction under typical pretreatment/reaction conditions. Due to the large number of possible atomic configurations, candidate structures were sampled by minima hopping with most stable structures selected for further discussion. CO_2 adsorption at various sites was investigated to probe the capability of the monomers/clusters to activate CO_2.

Our study sheds light on the ALD fabricated tertiary CZZ catalyst structure and proposes that contact between ZnO, Cu and ZrO_2 can promote methanol synthesis by the formation of CO_2 activation sites. We suggest that ALD is a suitable way to ensure that monomeric ZnO species are initially present, and that they are in contact with the Cu/ZrO_2 interface.

Computational Details

DFT calculations were performed using GPAW[43] employing the BEEF-vdW exchange–correlation functional.[44] The wavefunctions were treated in the projector-augmented wave (PAW)[45] formalism. The frozen-core approximation was applied for the core electrons of all elements. The global optimization of clusters was obtained via the minima-hopping (MH) method.[46] To enhance the computational efficiency and evaluate a large number of structures a double-ζ LCAO basis set was utilized in the MH calculations. Structures identified as minimum-energy candidates through MH were further optimized using a real-space grid basis with a maximum spacing of 0.2 Å and with spin-polarization. All calculations were periodic in the horizontal directions along the surface. Brilloiuin zone was sampled at the Γ point for the zirconia surface and Cu–ZrO_2 interface models, while a $4 \times 4 \times 1$ and $2 \times 2 \times 1$ Monkhorst-Pack k-point sampling mesh was applied to the Cu(111) and CuO(111), respec-

tively. Additionally, a Hubbard U correction[47] of 2.0 eV was applied to the d-orbitals of the zirconium atoms.[17,48] The geometry optimisations were performed using the Fast Inertial Relaxation Engine (FIRE) algorithm as implemented in the Atomic Simulation Environment (ASE).[49,50] Atoms in the bottom layers of surface slabs were fixed to their bulk positions (specific number of layers given below), while all other atoms were relaxed until the maximum residual force was reduced to less than 0.005 eV/Å. Partial charges on atoms were analysed Using the Bader partitioning method[51] using code developed by Tang et al.[52]

In this work, we employed a variety of zirconia supported single atom and cluster models. The composition of the $Zn_xCu_yO_z$ clusters was varied to include pure Cu and Zn as well as mixed metal clusters, reduced and oxidised clusters. The maximum total number of metal atoms in a cluster was 6. The zirconia surface was modelled with a m–$ZrO_2(\bar{1}11))$ surface slab that is two stoichiometric layers thick and built as a 2×2 supercell (32 Zr atoms, see Fig. S1). During optimisations, the bottom layers of the ZrO_2 slab was frozen in its bulk geometry. The $(\bar{1}11))$ surface of monoclinic zirconia is highly asymmetric with four identifiable Zr cation sites and a diverse selection of oxygen sites. A primitive repeating unit of the m–$ZrO_2(\bar{1}11))$ surface has 16 oxygens of which 5 are on the surface. Among these, four are 3-coordinated and located between Zr atoms and the remaining one is 2-coordinated, bridging two cations.

Additional calculations were performed for selected clusters adsorbed on a Cu(111) surface, an oxidic CuO(111) surface, and a Cu-ZrO_2 interface. The Cu(111) surface was modeled as a periodic three-layer-thick slab, 10.5 × 13.6 Å in size. (see Fig. S1). The bottom layer was fixed to bulk geometry during optimization. Cupric oxide (CuO) was identified as the major Cu phase in the as-prepared ALD catalyst.[8] The CuO(111) is the most stable surface of CuO in all but the most reductive conditions.[53] A three-layer-thick slab of CuO(111) was therefore used to model the oxidized Cu surface. The periodic computational cell measures 12.0 × 12.8 Å in size. Again, the bottom layer was kept in its bulk geometry. The initial CuO bulk structure was taken from the Crystallography Open Database[54–57] and

re-optimized computationally.

The stabilities of clusters were compared based on their formation energies. The formation energy ΔE_f of each cluster containing x Cu atoms, y Zn atoms and z O atoms is calculated according to Eq. 1 relative to the adsorbate–free m-$ZrO_2(\bar{1}11)$) surface, gaseous oxygen, and bulk metal. The formation energies of clusters on Cu(111) are calculated similarly with the appropriate substitutions.

$$\begin{aligned}\Delta E_f(\mathrm{Cu}_x\mathrm{Zn}_y\mathrm{O}_z/\mathrm{ZrO}_2) = {} & E(\mathrm{Cu}_x\mathrm{Zn}_y\mathrm{O}_z/\mathrm{ZrO}_2) \\ & - \left[E(\mathrm{ZrO}_2) + xe^{bulk}_{\mathrm{Cu}} + ye^{bulk}_{\mathrm{Zn}} + z\frac{1}{2}E(\mathrm{O}_2)\right]\end{aligned} \tag{1}$$

To circumvent the known inaccuracy of the DFT energy of a gas-phase oxygen molecule,[58–60] E_{O_2} was determined through the formation of water:

$$E(\mathrm{O}_2) = 2E(\mathrm{H}_2\mathrm{O}) - 2E(\mathrm{H}_2) - 2\Delta H^\circ_f(\mathrm{H}_2\mathrm{O}, T) \tag{2}$$

Using $\Delta H^\circ_f(\mathrm{H}_2\mathrm{O},\, 0\,\mathrm{K}) = 2.476\,\mathrm{eV}$ from the NIST-JANAF tables,[61] Eq. 2 gives $-32.997\,\mathrm{eV}$ for total energy of O_2 and the gas-phase error is $\varepsilon_{\mathrm{O}_2} = -0.83\,\mathrm{eV}$. This matches well with previously reported values of $-0.83\,\mathrm{eV}$ and $-0.81\,\mathrm{eV}$ for the BEEF-vdW functional.[58,59] Alternatively, when the amount of Zn and O is equal, the formation energy can be defined relative to bulk ZnO instead of bulk Zn and gas-phase O:

$$\begin{aligned}\Delta E_f(\mathrm{Cu}_x\mathrm{Zn}_y\mathrm{O}_z/\mathrm{ZrO}_2) = {} & E(\mathrm{Cu}_x\mathrm{Zn}_y\mathrm{O}_z/\mathrm{ZrO}_2) \\ & - \left[E(\mathrm{ZrO}_2) + xe^{bulk}_{\mathrm{Cu}} + ye^{bulk}_{\mathrm{Zn}} + z\frac{1}{2}E(\mathrm{O}_2)\right]\end{aligned} \tag{3}$$

However, we use Eq. 1 unless otherwise specified. The cohesive energy, ΔE_{coh}, of a cluster

is defined relative to isolated Cu, Zn, and O atoms adsorbed on ZrO_2.

$$\begin{aligned}\Delta E_{coh} = \; & [E(Cu_xZn_yO_z/ZrO_2) + (N-1)E(ZrO_2)] \\ & - [xE(Cu/ZrO_2) + yE(Zn/ZrO_2) + zE(O/ZrO_2)]\end{aligned} \tag{4}$$

N is the total number of atoms in a cluster. Equivalently, the cohesive energy can be calculated from formation energies:

$$\begin{aligned}\Delta E_{coh} = \; & \Delta E_f(Cu_xZn_yO_z/ZrO_2) \\ & - [x\Delta E_f(Cu/ZrO_2) + y\Delta E_f(Zn/ZrO_2) + z\Delta E_f(O/ZrO_2)]\end{aligned} \tag{5}$$

If a cluster has an equal number of Zn and O ($y = z$) atoms, cohesive energy can also be defined relative to adsorbed ZnO monomers on ZrO_2.

$$\Delta E_{coh,ZnO} = \Delta E_f(Cu_xZn_yO_z/ZrO_2) - [x\Delta E_f(Cu/ZrO_2) + y\Delta E_f(ZnO/ZrO_2)] \tag{6}$$

When assessing cluster agglomeration, it is also useful to calculate the energy relative to two existing clusters. For this, we can define a type of agglomeration energy using the formation energies of the clusters:

$$\Delta E_{agg} = \Delta E_f(AB) - (\Delta E_f(A) + \Delta E_f(B)) \tag{7}$$

where A and B refer to the constituent clusters of the agglomerate AB. The adhesion energy, ΔE_{adh}, of a cluster is calculated relative to the cluster in the gas phase.

$$\Delta E_{adh} = E(Cu_xZn_yO_z/ZrO_2) - [E(ZrO_2) + E^*(Cu_xZn_yO_z)] \tag{8}$$

where $E^*(Cu_xZn_yO_z)$ is the energy of the cluster, without the support but fixed in its adsorption geometry. The quantities above are defined equivalently on the Cu(111) surface

and the Cu/ZrO_2 interface.

Atomistic thermodynamics

DFT data was used as the starting point for the ab-initio thermodynamic treatment of the oxidation and reduction of small Cu/Zn clusters. The most thermodynamically stable oxygen content of each cluster is found by calculating the Gibbs energy of the oxidation reaction $\Delta G_r(T,p)$ for each z oxygen-containing cluster relative to the fully reduced cluster:

$$\mathrm{Cu}_x\mathrm{Zn}_y + \mathrm{z}\frac{1}{2}\mathrm{O}_2 \longrightarrow \mathrm{Cu}_x\mathrm{Zn}_y\mathrm{O}_z \tag{R2}$$

$$\Delta G_r(T,p) = E(\mathrm{Cu}_x\mathrm{Zn}_y\mathrm{O}_z/\mathrm{ZrO}_2) - [E(\mathrm{Cu}_x\mathrm{Zn}_y/\mathrm{ZrO}_2) + z\mu_\mathrm{O}(T,p)] \tag{9}$$

This examination is equivalent to the one in ref. 33 as well as energies of O adsorption used in ref. 62 but calculated per cluster as opposed to surface area. Vibrational energy contributions of surface-bound clusters to the free energies were assumed to be minimal. Therefore, DFT energies were used for the clusters instead of Gibbs free energies. Temperature and pressure effects were included in the chemical potential, $\mu_\mathrm{O}(T,p)$, of oxygen. The contribution of temperature to the standard chemical potential of O_2 $\Delta\mu^\circ(T)$ was calculated using experimental values for $H-H^\circ(T_r)$ and S° taken from the NIST JANAF thermochemical tables.[61]

$$\begin{aligned}\Delta\mu^\circ(T) &= \Delta H^\circ + T\Delta S^\circ \\ &= [H^\circ(T) - H^\circ(T_r)] - [H^\circ(0\,\mathrm{K}) - H^\circ(T_r)] - T \times [S^\circ(T) - S^\circ(0\,\mathrm{K})]\end{aligned} \tag{10}$$

We define the change in chemical potential relative to 0 K)

$$\Delta\mu(T,p) = \Delta\mu^\circ(T) + k_\mathrm{B}T\log\frac{p}{p^\circ} \tag{11}$$

And thus the chemical potential of a gaseous oxygen is:

$$\mu_O(T,p) = \frac{1}{2}E(\mathrm{O_2}) + \Delta\mu_O(T,p) \tag{12}$$

where O_2 energy includes the correction according to Eq. 2. To estimate the chemical potential of oxygen under the highly reductive conditions typically used for CO_2 conversion, we applied the balance of molecular hydrogen and water gas: $\Delta\mu^\circ_{\mathrm{O}} = \Delta\mu^\circ_{\mathrm{H_2O}} - \Delta\mu^\circ_{\mathrm{H_2}}$

Results and Discussion

We focus on small sub-nanometer clusters, each comprising up to 8 Zn and Cu atoms supported on m–ZrO_2 (0–4 Zn, 0–4 Cu, including mixtures of the two). Selected clusters underwent further examination on Cu(111) and CuO(111) surfaces as well as a Cu-ZrO_2 interface. Beyond metal-only clusters, we generated and optimized clusters with varying amounts of oxygen. Consequently, the smallest systems consisted of single Cu or Zn atoms, while the largest cluster was $Cu_4Zn_4O_4$.

ZrO_2 supported $Cu_xZn_yO_z$ clusters

In the ALD prepared CZZ systems, the Cu and ZnO components are added to the zirconia support by incipient wetness impregnation (IWI) and ALD, respectively.[8] In the case of the best performing sample, the ALD step is performed last, which should ensure that some of the ZnO units are initially present on the ZrO_2 support and not covered by Cu. All minimum-energy structures optimized on monoclinic zirconia are presented in the supporting information Fig. S2 for Cu_xO_z and Zn_yO_z clusters, and S3 for mixed $Cu_xZn_yO_z$ clusters.

Zn_yO_z clusters

Recent studies[8,18] that have used ALD for catalyst preparation have suggested that Zn exists approximately as atomically dispersed species on the surface of the as-prepared catalyst.

Depending on their mobility and relative stability on the surface, the monomers could migrate and eventually react together to form sub-nanometer clusters. Given the varying reaction conditions the catalyst experiences during synthesis, pre-treatment, and operation, ranging from highly oxidizing to very reductive, we considered both metallic Zn_y clusters as well as oxidized Zn_yO_z clusters. We consider the ZnO monomer as the reference system, rather than separate Zn and O units, as it is the assumed form of the as-prepared ALD Zn units.

In the most stable configuration, the ZnO monomer binds to a 2-coordinated oxygen site on the ZrO_2 surface through the formation of a Zn–O bond. The oxygen atom of the monomer binds to a Zr top site. Adsorption at the low-coordinated O site is 1.5 eV stronger than the best geometry found for binding to a 3-coordinated oxygen, and the ZnO monomers relax to the 2-coordinated site almost independent of the starting geometry. This points to the maximum coverage of 2.24 ZnO monomers per nm^2, which is comparable of 1.9 Zn/nm^2 determined experimentally for ALD-prepared Zn/ZrO_2.[8] The formation energy of the most stable ZnO monomer is endothermic (+0.74 eV) relative to ZnO bulk. The adhesion energy is −4.40 eV, and the cohesion energy relative to Zn and O ad-atoms is −1.51 eV. The same coordination site and similar binding strength has been previously found for sintering-resistant RuO monomers on monoclinic ZrO_2.[63] In general, sub-nanometer Zn_yO_z clusters tend to attach to the ZrO_2 support by bonding to the surface oxygens through the Zn atoms, particularly those with lower coordination. Additional oxygen atoms introduced as part of the clusters create extra contact points by bridging surface Zr cations and the Zn atoms within the cluster. In cases where possible, $Zn^{\delta+}$ centers form planar, trigonal ZnO_3 moieties with surface and cluster oxygens. The geometric arrangement is also observed in the Zn_2O cluster, where one Zn atom is part of the trigonal shape rather than an oxygen. This type of trigonal motifs have also previously been identified in Cu(111)-supported Zn_yO_z clusters.[33] However, many nearly linear O–Zn–O moieties are also identifiable, as exemplified by Zn_2O_2. It is noteworthy, that oxygen atoms act as bridges between Zn centers, although $Zn^{\delta+}$ can also directly form bonds with one another, as seen in Zn_2O and Zn_3O_2. Stoichiometric 1:1

Zn:O clusters are the most stable and all show $E_f = -1.35$ per atom whereas removing or adding oxygen makes the clusters progressively less stable. In some over-oxidized clusters two oxygens can form O–O bonds, resembling an adsorbed O_2 molecule. For an example, see Zn_3O_4 in Fig. S2. When the cluster size increases, the cohesive energies of stoichiometric $(ZnO)_n$ clusters are close to 0 eV with respect to ZnO monomers on zirconia (see Table S1). Therefore no clear thermodynamic driving force is present for the formation of oxidized ZnO sub-nano clusters (see Fig. 2). There exists, however, still the tendency towards bulk ZnO formation, as can be seen by the positive formation energies in Table S1.

The possibility of Zn monomer species to exist as reduced metal ad-atoms, e.g. due to highly reducing conditions, was also considered. The single Zn ad-atom is most stable on a Zr cation top site where it settles above the surface at a Zr–Zn distance of ≈ 3.5 Å. The variation in energy between all Zr sites available is less than 0.1 eV. Metallic 2–4 atom Zn clusters have structures where Zn atoms are similarly located on Zr top sites. These Zn_y clusters display longer Zn–Zn distances than bulk Zn, decreasing the distance with increasing cluster size. Fig. 1 shows that Zn_3 and Zn_4 take trigonal shapes with the latter being in a pyramidal form, although a planar rhombic Zn_4 is only 0.1 eV less stable. These geometries are similar as those previously reported for small Rh clusters on m–ZrO_2,[29] with the exception that Rh_2 shows no significant Rh–Rh bond elongation compared to bulk Rh. Notably, the formation energies of the most stable Zn ad-atom and metallic clusters are endothermic by 0.6 eV per cluster atom (see Table S1) which is very close to that of the ZnO units described above but significantly less endothermic than the +2.1 eV value we calculated for a Cu atom. The formation energies of metal ad-atoms are typically strongly endothermic.[29,31] Here we find that while there is ultimately a thermodynamic driving force for large Zn particle growth, the initial stages of agglomeration are nearly thermoneutral (Fig. 1).

Despite zirconia's tendency to resist reduction, several studies have shown evidence for the formation of oxygen vacancies on its surface either near metal–zirconia interfaces or single metal sites.[48,64–66] The oxygen vacancies formed have been found to enhance adsor-

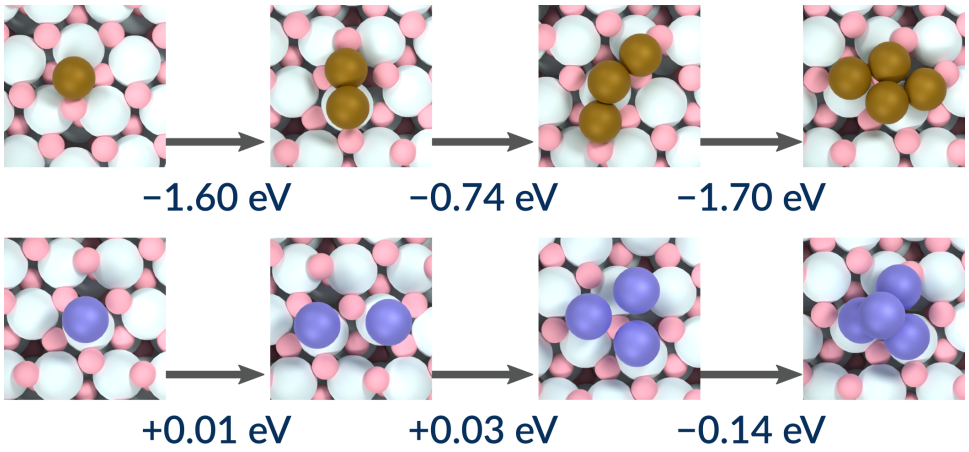

Figure 1: Stepwise energy differences of building a cluster from adsorbed atoms at infinite separation during the initial stages of Cu_x and Zn_y agglomeration. Brown: Cu, purple: Zn.

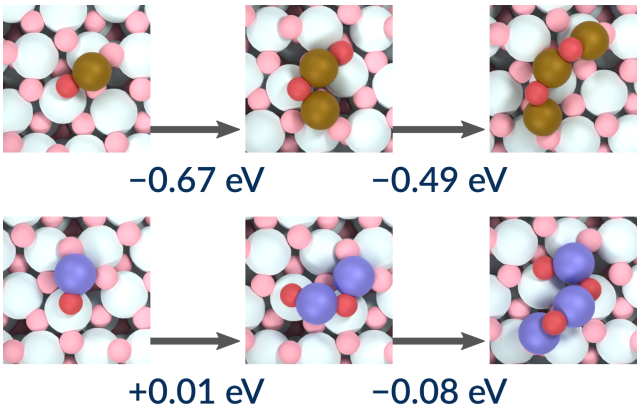

Figure 2: Stepwise energy differences of building a cluster from adsorbed atoms at infinite separation during the initial stages of Cu_xO_z and Zn_yO_z agglomeration. Brown: Cu, purple: Zn, red: O.

bate binding[67,68] to ZrO_2 and suggested as the cause for increased activity towards CO_2 conversion.[64] They are also known to act as anchor sites that can stabilize single-atoms on catalyst surfaces.[29,69] We therefore addressed how the ZnO promoter binds to ZrO_2 surface vacancies. Previous computational studies have found that the vacancy formation energy is the least endothermic for the 2-coordinated oxygen on the m–$ZrO_2(\bar{1}11)$) surface.[63,68,70] Therefore, we chose it as the model vacancy site for $Cu_xZn_yO_z$ binding. As can be seen from the relative energies in Table S4, oxygen vacancies on the ZrO_2 surface bind all clusters stronger than the pristine zirconia surface, often by several eV, and can thus act as anchors. Furthermore, oxygen-containing clusters are stabilized more than reduced clusters. Notably, non-oxidized Zn and Zn_2 show the smallest differences, only being stabilized by ≈ 0.5 eV. A ZnO monomer that is captured by an oxygen vacancy can spontaneously donate its oxygen to fill in the vacancy, breaking the Zn–O bond in the process (see Fig. S5). Other oxygen-containing clusters, as well as the CuO monomer, donate an oxygen to fill the vacancy but are not dissociated in the process. In these cases, then, the binding geometries are effectively the same as the binding of a cluster with one less oxygen on pristine ZrO_2.

Mixed clusters

Although copper tends to form larger nanoparticles on the zirconia surface, the formation of mixed clusters with Zn cannot be ruled out, as the thermodynamic feasibility of mixing Cu and Zn is evident based on the computed formation energy of BCC-packed CuZn (α-brass) being -0.16 eV per CuZn unit. Experiments also demonstrate the possibility of Cu-Zn (nano)alloys formation when the conditions become reductive.[24,39–42] Although multiple studies point to ZnO being the more stable state under the high-pressure reaction conditions,[24,26,71] other works have attributed a high activity for CO_2 conversion to alloyed/metallic Zn sites on the catalyst surface.[3,42,72,73] Our investigation delves into the interaction between ZnO sub-nano structures, present in the as-prepared catalyst, and Cu particles. The aim is to understand whether stable Cu and Zn mixtures could form un-

der reaction conditions. This scheme describes the thermodynamic feasibility of a process where small copper species detach from large Cu nanoparticles to react with ZnO species not initially in contact with the copper component of the catalyst. Ultimately, such a process would also depend on kinetics of Cu particle disintegration (e.g. via the Ostwald ripening process[31]) and migration of Cu species, which is beyond the scope of the present study. The stability of reduced and oxidized Cu_xO_z clusters was also determined as they could exist as transient species during the agglomeration process, and besides serve as reference systems for the stability of the mixed clusters.

A single Cu ad-atom binds to the 2-coordinated oxygen site of the zirconia surface. Small Cu_x clusters are similarly attached to the surface via Cu–O bonds and take flat or linear shapes, which maximize oxygen contact (see Fig. 1). As expected, the growth of Cu particles is thermodynamically favourable. Generally, mixed Cu_xZn_y clusters take similar shapes and placements as Cu_x clusters of the same size do and are geometrically flat, maximizing contact with the support. Similarly, oxidized mixed clusters bear a large resemblance to Cu_xO_z and Zn_xO_z structures. All clusters exhibit a tendency to bind to low-coordinated oxygen sites in both their reduced and oxidized forms. The structures are generally more stable when a maximal number of their oxygens are in contact with the zirconia surface. However, when multiple oxygens are present in the cluster, this effect is restricted by internal forces within the cluster and thus some oxygen stays out of contact with the support. Internally, Zn–Zn bonds are uncommon in mixed clusters and the zincs are typically separated by Cu and O atoms in the lowest-energy configurations. The structures of mixed clusters on ZrO_2 can be seen in Fig. S3. Figure 3 shows the initial stages of the agglomeration of non-oxidized mixed clusters. At each step, the agglomeration is energetically favourable. However, after the initial combination of Cu and Zn, the agglomeration energies of additional Zn atoms become clearly less negative, mirroring the case of Zn_y clusters. In situations where an individual Zn ad-atom can combine with a Zn_y or Cu_x cluster, the formation of a mixed cluster is thermodynamically favoured over the formation of a pure Zn cluster (see

Fig S6). Furthermore, while ZnO monomers do not show a clear tendency to create Zn_yO_y agglomerates, the formation energies of mixed metal clusters (Table S1) show that mixing with copper could provide an alternative route for initial stage agglomeration. However, to verify this would require further computational and experimental investigations into the mechanism and kinetics of Cu particle disintegration/agglomeration.

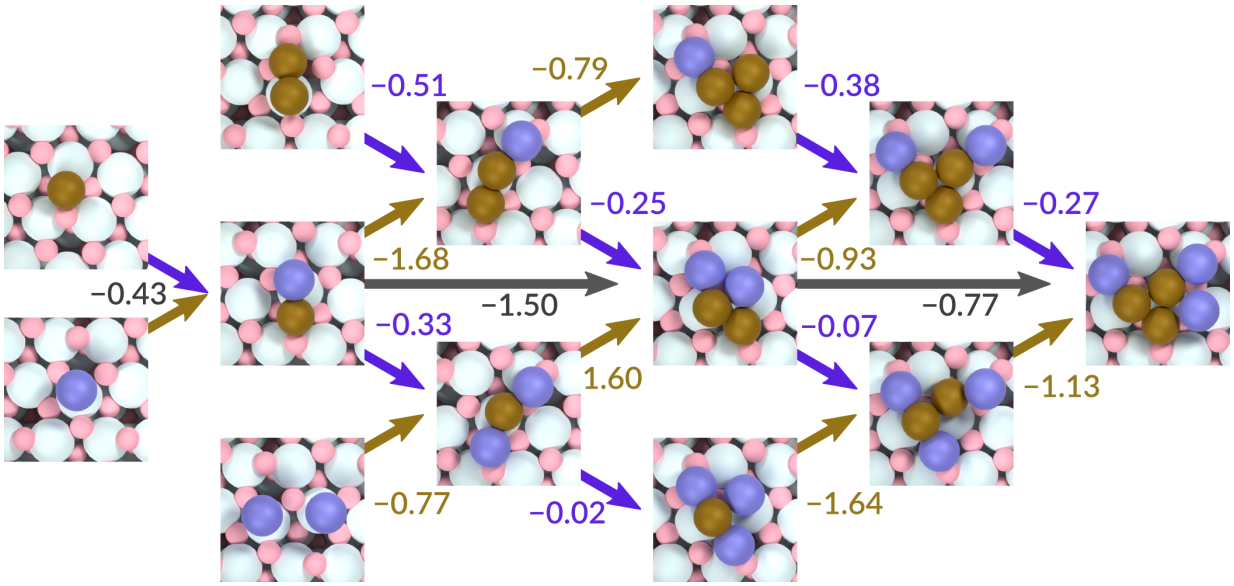

Figure 3: Stepwise agglomeration of mixed, non-oxidized Cu_xZn_y clusters from Cu, Zn, and CuZn units adsorbed on ZrO_2. The numbers are agglomeration energies (Eq. 7) in eV associated with introducing a Cu (up), Zn (down) or CuZn unit (horizontal) from infinite separation into the cluster. Brown: Cu, purple: Zn.

Clusters on Cu surfaces

During catalyst preparation and CO_2 hydrogenation, small Zn or ZnO deposits may also form on larger Cu nanoparticles—either due to the chosen preparation method, such as ALD.[8,18] Although a reaction between the Zn(acac) and copper has not been explicitly demonstrated, in principle some of the ZnO units could be deposited on the copper particles as well as the ZrO_2 support, when the ALD step is performed after IWI. Alternatively, strong metal–support interaction between Cu and ZnO has been suggested to result in the migration of the ZnO component to form an overlayer on top of the Cu component.[26,74,75] However, a

previous study has asserted that Zn may need to be in its reduced form for substantial migration of Zn on top of Cu particles to occur.[74] Interfaces between ZnO islands and Cu particles are proposed as active sites for CO_2 adsorption and activation in a Cu/ZnO($/Al_2O_3$) system.[2,15,18,35,76] Consequently, Cu–ZnO interaction can also contribute to the activity in ternary CZZ systems. To explore this further, several Cu_xO_z and Zn_yO_z clusters (see Table S2 and Fig. S4) were optimized on a Cu(111) surface, representing a scenario where they are positioned on top of larger metallic Cu particles.

The geometries of the optimized Zn_yO_z clusters on Cu(111) are presented in Fig. S4. Metallic Zn clusters are more stable on the Cu surface than they are on zirconia. However, both their formation and cohesive energies approach effectively zero, showcasing a behaviour opposite that on the zirconia surface, where the formation of ZrO_2-bound Zn atoms is endothermic. The average Zn–Zn distance in unoxidized clusters is 2.7 Å and comparable to that of bulk Zn as well as the Cu–Cu distance of the underlying surface agreeing well with the previously reported value.[33] Moreover, the study reported only marginal energy differences between reduced Zn_y clusters of various shapes. These results suggest that the energy benefit of forming a Zn_y cluster structure is relative small. The ZnO monomer and Zn_yOz clusters show similar structural motifs as were seen on a zirconia surface. These motifs are the same as were identified in a recent study[33] and the structures found here are very similar. Binding to the Cu surface happens through both Cu–O and Cu–Zn bonds. Calculating the difference in the formation energies, ΔE_f given in Table S2, for each cluster on ZrO_2 and Cu(111) allows us to determine whether adsorption is more favorable on a metal or oxide surface. The formation energies of Zn_yO_z species on a Cu(111) surface are 0.5 to 0.9 eV less negative compared to equivalent clusters on zirconia. Therefore, there is a thermodynamic tendency for oxidic Zn to migrate onto the zirconia support if it is formed on the Cu surface during catalyst preparation. Conversely, the migration of ZnO units from the zirconia surface to the Cu is thermodynamically unlikely. Non-oxidized Zn_y particles are generally more stable on Cu(111) by ≈ 0.6 eV per Zn.

Cupric oxide has been identified as the primary oxidized Cu phase in as-prepared catalysts produced using ALD prior to reductive pre-treatment.[8] Hence it is pertinent to examine the binding of ZnO on CuO(111). Two zinc-oxygen clusters, ZnO and Zn_2O_2, were considered as representatives of the highly dispersed small ZnO species that have been suggested to exist in the as-prepared catalyst after ALD.[8,18] The ZnO monomer favors a horizontal geometry with Zn binding to a surface oxygen and O to a Cu top site. The ZnO formation energy is $\approx +1.6$ eV on CuO(111) being only slightly higher than on Cu(111) but significantly more endothermic than on ZrO_2. This indicates that ZnO monomers are thermodynamically more stable on the ZrO_2 support than Cu particles, regardless of Cu oxidation state. The ΔE_{agg} of two ZnO monomers combining on CuO(111) is exothermic by -1.08 eV, showing that agglomeration is similarly favourable as it is on Cu(111).

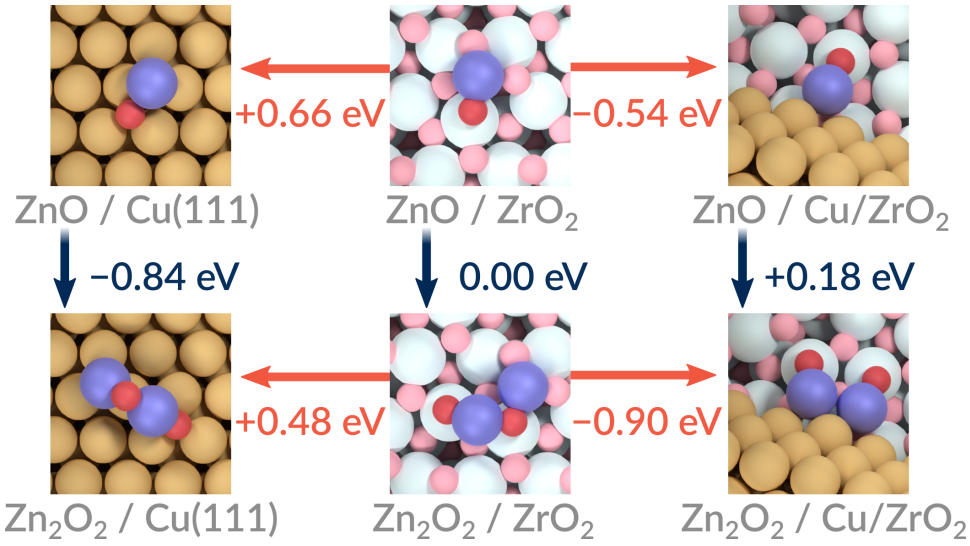

Figure 4: Blue arrows represent the energy differences of building a Zn_2O_2 cluster from two infinitely separated ZnO units on each support. Orange arrows depict diffusion of the cluster to different sites on the surface of a CZZ catalyst. The orange energy values are relative to the cluster on zirconia. Brown: Cu, purple: Zn, red: O. Lighter colored atoms are part of the support.

Clusters at interface

The interfaces forming between Cu particles and the supporting ZrO_2 play a crucial role in multi-component systems, potentially displaying unique activity. Numerous computational studies have underscored the importance of the Cu–ZrO_2 interface as an active site for CO_2 activation and hydrogenation.[13,17,77,78] Consequently, it is reasonable to investigate the behaviour of ZnO promoters in this context. We calculated the stability of the ZnO and Zn_2O_2 units at the Cu–ZrO_2 interface, using a supported nanorod model from our previous studies.[17,78] Fig. 4 displays the most favourable ZnO and Zn_2O_2 binding structures at the Cu-ZrO_2 interface showing that Zn interacts with Cu rod and O binds to the Zr cation. The relative energies in Fig. 4 demonstrate that the ZnO unit is 0.54 eV more stable at the interface than on the ZrO_2 surface and 1.20 eV more stable than on the Cu(111). While ZnO agglomeration is thermoneutral on ZrO_2, it is unfavorable at the interface, as indicated by the endothermic agglomeration energy of +0.18 eV for Zn_2O_2 formation from two ZnO units.

In summary, binding of ZnO monomers is stabilized by the Cu–ZrO_2 interface, leading to a thermodynamic tendency for them to migrate from Cu and ZrO_2 surfaces and into interfacial areas. While the Cu(111) surface is the least stable support for Zn_yO_z species to bind to, it is the most favorable location for their agglomeration. Conversely, initial ZnO agglomeration is thermoneutral on zirconia and slightly endotermic at the Cu–ZrO_2 interface. It should be noted that this thermodynamic examination can not take into account the possible kinetic barriers of cluster diffusion on Cu and ZrO_2 surfaces or across a metal–oxide interface. Methods such as mean-field or Monte Carlo microkinetic modeling[79] and ab initio molecular dynamics (MD) simulations[80] could be used to gain further understanding of the rate of agglomeration/sintering.

Cluster composition under reaction conditions

The extent of reductive or oxidative conditions varies widely between catalyst preparation steps and the operation conditions for CO_2 conversion to methanol. During synthesis, the catalyst undergoes an oxidative pretreatment, such as heating under synthetic air (80 % oxygen).[8] On the other hand, the CTM reaction is carried out under high pressures ranging from 10 to 50 bar in a mixture of typically 1:3 CO_2 and H_2.[2] Despite extensive research efforts, the precise oxidation state of Zn under reaction conditions remains a source of debate.[2,3,12,15,24,26,36,40,72,73,81–84] As has been noted before,[24,26,40] the disparate results can largely be explained by the diverse conditions and the pressure gap between catalyst preparation, ex situ characterization studies, and the reaction conditions. To address this ambiguity, we employ atomistic thermodynamics to assess the stability of both reduced and oxidized clusters at conditions relevant to catalyst pre-treatment and CO_2 conversion to methanol.

As the phase diagrams presented in Figures 5 and S7 illustrate, small Zn clusters adsorbed on zirconia exhibit greater stability in their oxidized forms—even under the highly reductive reaction conditions of CO_2 hydrogenation to methanol. As the initial agglomeration of ZnO on ZrO_2 is practically thermoneutral, the promoter may be present in a wide variety of sizes ranging from ZnO monomers to larger clusters. However, the stoichiometric 1:1 composition (Zn_yO_y) proves to be the thermodynamically most stable form among all the Zn_yO_z clusters considered, both in the reductive atmosphere used in CTM as well as conditions corresponding to the oxidative pretreatment that is a part of catalyst preparation. We note that the Gibbs energies of oxidation are often very close to one another (eg. Fig. 5 a)). Therefore, while the most stable compositions at each oxygen chemical potential are highlighted, in reality many states may exist as an ensemble. The activation barriers of oxygen gas adsorption or the $Zn + H_2O \leftrightarrow ZnO + H_2$ process were not studied here but may bring further nuance to the situation as the reduction or oxidation of certain clusters could be kinetically limited. As Figure 5 b) shows, the Gibbs free energy of formation becomes increasingly more negative for larger cluster sizes at oxidizing conditions. The differences in

ΔG_f become smaller as the temperature increases. A similar trend with respect to temperature has been previously observed for Zn_yO_z clusters on Cu(111).[33] However, we find that at the methanol synthesis reaction conditions the difference between monomers and larger clusters is non-existent or even reversed. This indicates that monomers may be more able to resist agglomeration during the reaction as opposed to during the oxidizing pre-treatment. For all conditions, the formation free energy change is monotonic.

The oxidation characteristics of Cu small clusters are more diverse. Under oxidative conditions, Cu clusters again display the highest stability in a stoichiometric composition (see SI Fig. S8). However, in a reductive atmosphere, a single Cu atom adsorbed on zirconia is more likely to exist as an ad-atom with no additional oxygen. For Cu_2 and Cu_3 clusters, the thermodynamics favor partial oxidation. However, the oxidation energies of different cluster compositions can be very similar. In particular, Cu_3O_z clusters are all no more than 0.3 eV apart in the range of typical reaction conditions. The partial oxidation of small Cu_x units is preferred, in contrast to the stoichiometric oxidation of Zn_yO_y. This is consistent with bulk oxide formation energies: CuO formation energy is -1.48 eV and for ZnO it is -3.47 eV relative to bulk metal and gas-phase oxygen. This, together with the considerable agglomeration and cohesive energies of Cu_z clusters, is consistent with experimental results that have generally identified large Cu deposits with a significant amount of reduced Cu.[8,85–87] The redox properties of mixed $Cu_xZn_yO_z$ clusters primarily resemble those of small Zn clusters in that completely metallic clusters are thermodynamically unfavored (see Fig. S9). However, the oxygen content per metal atom varies. The ab-initio thermodynamics indicate that metallic alloy clusters are not stable under reaction conditions, although there is a possibility of forming mixed oxidized clusters.

CO_2 adsorption and activation

Methanol synthesis requires the activation of the inert CO_2 molecule on the catalyst surface. Activation may take place through adsorption and bending of the molecule, followed by dis-

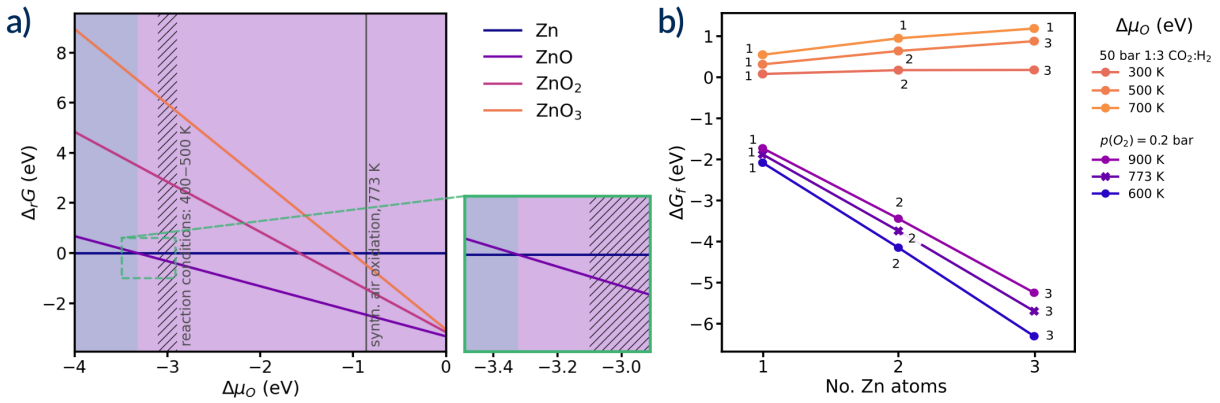

Figure 5: a) Phase diagrams showing the relative stabilities of Zn_1O_z species with different oxygen content (from Eq. 9) as a function of oxygen chemical potential. Colored lines corresponding to each cluster show their energies relative to the fully reduced cluster and gas-phase O_2. The background is colored according to the lowest-energy state for ease of identification. Oxygen chemical potential relevant to pre-tretment and CTM reaction conditions are indicated with vertical lines and regions with diagonal hatching, respectively. b) Formation energies at several oxygen chemical potentials in the regions of the reaction and oxidative pretreatment conditions. The values of ΔG_f are calculated according to Eq. 1 by substituting μ_O for $\frac{1}{2}E(O_2)$. The numbers inside the graphs indicate the number of oxygen atoms in the most stable structures.

sociation or hydrogenation. The bent adsorption configuration could be e.g. a $CO_2{}^{\delta-}$ on a metal surface, or a carbonate-like $CO_3{}^{2-}$ on a metal oxide, which both require charge transfer from the catalyst to the molecule. The computed formate pathways on metal surfaces often imply that CO_2 activation occurs through direct reaction between linear CO_2 and a dissociated hydrogen species on the surface.[3,4,15,87] In previous studies,[13,17,77,78] it has been found that the Cu/ZrO_2 interface is capable of adsorbing and activating CO_2, enabling the surface reaction between adsorbed bent CO_2 species and hydrogen to produce a carboxyl (COOH) instead of formate. In line with the previous studies,[3,4,17,77,88] we find that a (111) facet of Cu weakly physisorbs CO_2 in a linear, non-activated configuration, with an adsorption energy of -0.21 eV. On ZrO_2, CO_2 adsorbs in a trigonal, carbonate-like geometry, wherein the carbon atom coordinates to a ZrO_2 lattice oxygen and the oxygens of the adsorbate rest on $Zr^{\delta+}$ sites. The most favourable adsorption site is the 2-coordinated lattice oxygen, where $E_{ads} = -0.62$ eV. However, one fifth of surface oxygens are 2-coordinated and the adsorption energies to other sites are only mildly exothermic varying from -0.09 eV to -0.16 eV.

When adsorbed, the CO_2 takes a small negative charge of $-0.20e$, which is in the same order as has been determined before.[13] Previous computational studies using diverse models for Cu-ZrO_2 interfaces[13,17,77,78] indicate that CO_2 adsorbs at a Cu-ZrO_2 interface in a bent geometry. In our previous study, we found that CO_2 attaches to the Cu component through the carbon atom with both oxygens binding to the nearest Zr cations.[17] The adsorption energy is -0.63 eV, which is comparable to that at the most stable adsorption site on ZrO_2. Our earlier work demonstrated that incorporating Zn into the Cu matrix at the interface can strengthen CO_2adsorption by up to 0.66 eV compared to the Cu-only interface.[17] Here, we investigate CO_2 adsorption on ZnO monomers on ZrO_2, Cu(111), and the Cu-ZrO_2 interface to further quantify the promoting effect of ZnO.

Fig. 6 illustrates CO_2 adsorption geometries and energies at potential active sites on a Cu/ZnO/ZrO_2 catalyst, particularly when ZnO is deposited with ALD. In the preferred binding configuration on the zirconia supported ZnO, CO_2 forms bonds between its carbon atom and the oxygen of the ZnO monomer, and between its oxygen atoms and Zr surface cations. The adsorption energy of -0.69 eV is only slightly more negative than the most stable adsorption geometry on promoter-free ZrO_2. In contrast to a bare Cu(111) surface, CO_2 bound to the oxygen atom of a ZnO unit on Cu(111) is clearly activated and stable featuring an adsorption energy of -0.42 eV. The activation is evident from the carbonate-like structure which is similar to that observed on zirconia. CO_2 bound to ZnO has a slight negative charge of $-0.20e$—the same as the charge of a CO_2 molecule adsorbed on ZrO_2 in a carbonate geometry (see SI Table S5 for atomic charges). The dispersion of Zn_yO_z units on Cu particles can increase the number of sites where activated CO_2 interacts with the Cu catalyst. This could facilitate the reaction between the adsorbed CO_2 and the dissociated hydrogen that is produced on Cu particles. Previous computational studies have similarly explored CO_2 adsorption to ZnO clusters on copper surfaces. For example, one study modeled the ZnO/Cu interface using a hydrogen-terminated $Zn_6O_7H_7$ cluster model.[15] In this case, CO_2 adsorption and activation was achieved at the edge of the cluster

with the molecule binding to the Cu surface through its carbon and to the cluster through its oxygen. However, the binding energy was found to be endothermic by +0.47 eV, making it unfavourable. The disparity in CO_2 adsorption energy between this model and ours is likely explained by their inclusion of the H termination, which reduces the reactivity of the cluster towards CO_2 activation. Another study using a graphitic-like ZnO layer model supported on a Cu(111) surface suggested that the adsorption CO_2 to ZnO edges was facilitated by the presence of oxygen vacancies in the zinc oxide.[18] At the vacancy site, CO_2 binds to the ZnO layer through both a carbon and an oxygen atoms with an adsorption energy of −0.56 eV. However, we find that stoichiometric ZnO monomers also act as efficient adsorption sites.

While the Cu–ZrO_2 interface is already capable of activating CO_2, ZnO units that have migrated to the interface can also serve as sites for CO_2 adsorption and activation. In the most stable structure, the molecule again binds to the oxygen of the ZnO unit, forming the familiar carbonate-like structure and taking a negative charge of $-0.29e$. The oxygens originally belonging to the molecule reside on the zirconia surface, mirroring their positioning during adsorption to the interface without ZnO. The corresponding adsorption energy of −1.60 eV indicates significantly stronger adsorption compared to adsorption at the simple Cu–ZrO_2 interface (−0.63 eV) and somewhat stronger than adsorption at mixed CuZn–ZrO_2 interfaces (−1.1 eV to −1.3 eV).[17] It is also markedly stronger than CO_2 adsorption to zirconia alone. The atomic charges in the ZnO-bound CO_2 are similar on Cu and ZrO_2 surfaces and the interface. Therefore, the enhanced binding is not simply explained by charge transfer. Instead, it may be due to the conformational flexibility of the ZnO monomer at the interface, which allows a bidentate binding geometry and a lower geometric strain for the formed CO_3 moiety. Nevertheless, this demonstrates that dispersed Zn can have a substantial impact on CO_2 binding at Cu/ZrO_2 interfaces, regardless of its oxidation state. In a recent computational study,[16] the ZnO/Cu and ZrO_2/Cu interfaces were modeled using a $Zn_1Zr_2O_3$ cluster model deposited on Cu(111). This model effectively activated and bound CO_2, with the molecule coordinated to the Zr center of the cluster through an oxygen. The adsorption

energy of −1.07 eV falls within the same range as the aforementioned CuZn–ZrO_2 interfaces. However, the authors report significantly weaker binding ($E_{ads} = -0.17$ eV) on the ZnO/Cu side of the cluster.

After the successful adsorption of CO_2, the reaction can continue through a formate (HCOO) intermediate or via the reverse water-gas shift pathway (COOH intermediate) and eventually into methanol. A recent computational study[89] examining the binding of CO and CO_2 at a Cu/MgO interface determined the binding free energy of CO_2 to be −0.36 eV. It was suggested that at this stage, the adsorption may be strong enough to lead to catalyst poisoning and thus reduced conversion activity. While the free energies of the adsorbed molecules were not determined here, the strongly exothermic CO_2 binding to ZnO monomers as well as the known stability of HCOO on zirconia[13,17,77] may pose similar challenges if the barriers for further hydrogenation steps are high. In the past, the intermediates networks along both pathways have been studied on zirconia, Cu/CuZn surfaces, and metal–oxide interfaces.[3,4,13,15,17,77] From these results, one can conclude that certain sites are more optimal for the binding of different reaction intermediates, as some (such as COOH) adsorb more strongly to the Cu–ZrO_2 interface, while others (such as HCOO) bind on the ZrO_2 alone. While the binding of further intermediates and the elementary reactions between them were not a part of this study, the Zn_yO_z species described here may also act as favourable active sites for later hydrogenation steps.

Conclusions

Our results show that monomeric ZnO units are resistant to initial stages agglomeration on the zirconia surface, as there is no significant thermodynamic driving force to form small clusters. Instead, alloying ZnO with copper single-atoms is a thermodynamically feasible pathway for particle growth, which could result in mixed metal particles of varying degrees of oxidation. Ab initio thermodynamic analysis shows that even under the reducing methanol

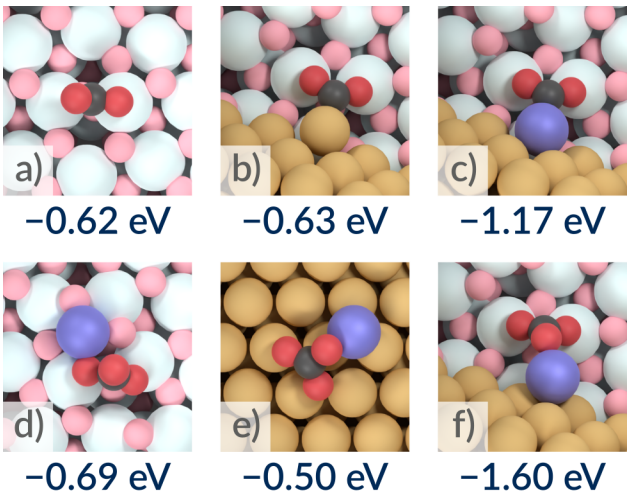

Figure 6: CO_2 adsorption energies on different supports and Zn-promoter sites: a) ZrO_2, b) Cu–ZrO_2 interface, c) CuZn–ZrO_2 interface (Zn-poor), d) ZnO/ZrO_2, e) ZnO/Cu(111), f) ZnO/Cu–ZrO_2.

synthesis conditions the ZnO and mixed ZnO/Cu clusters are not completely reduced. Formation free energies imply that ZnO monomers could be more resistant to agglomeration at the reaction conditions as opposed to oxidizing pre-treatment conditions. Furthermore, ZnO migration to the copper-zirconia interface is thermodynamically favourable, whereas migration to the extended Cu nanoparticle (111) facets is not preferred. However, ZnO clustering is more feasible on the copper surface. If ZnO species present on Cu are large enough (beyond the sizes explored in the present work), they may be able to resist migration to the interface and the support. Our results do not therefore rule out the presence of larger structures, such as ZnO islands, on the copper particles especially for larger ZnO loadings.

Small ZnO clusters are able to adsorb and activate CO_2 on ZrO_2, Cu(111) and the Cu–ZrO_2 interface. CO_2 binding is strongest at the Cu–ZrO_2 interface where dispersed ZnO promoter units are also thermodynamically most stable and resistant to forming larger ZnO structures. The Cu-ZnO-ZrO_2 interface offers stronger adsorption than the promoter-free Cu-ZrO_2 or nanoalloyed CuZn-ZrO_2 interfaces. ZnO dispersed on the surface of a Cu particle may also offer sites where CO_2 can be activated upon adsorption, as opposed to the physisorption typical of Cu surfaces. Our results offer an atomic-level look at the behaviour

of the hypothesized highly dispersed ZnO on a zirconia support and the origin of their promoting effect.

Acknowledgement

We thank Prof. Riikka Puurunen and her research group for fruitful discussions on ALD in catalysis and in CTM chemistry. The work was funded by Academy of Finland (project 329977). A.L. also acknowledges a kind grant by the Vilho, Yrjö, and Kalle Väisälä Foundation of the Finnish Academy of Science and Letters. Electronic structure calculations were carried out using computational resources provided by the CSC — IT Center for Science, Espoo, Finland (https://www.csc.fi/en/) and computer capacity from the Finnish Grid and Cloud Infrastructure (urn:nbn:fi:research-infras-2016072533).

Supporting Information Available

See supporting information for illustrations of global minimum energy structures, a full list of formation-, adhesion-, and cohesive energies, additional figures for the atomistic thermodynamics of $Cu_xZn_yO_z$ species, and atomic charges in CO_2 adsorption geometries. The computed structures presented in this study are openly available to download from the Finnish Fairdata service at `https://doi.org/10.23729/81cea552-50db-47b9-ac58-477977cbc71d`.

References

(1) Tackett, B. M.; Gomez, E.; Chen, J. G. Net reduction of CO_2 via its thermocatalytic and electrocatalytic transformation reactions in standard and hybrid processes. *Nat. Catal.* **2019**, *2*, 381–386, DOI: 10.1038/s41929-019-0266-y.

(2) Kattel, S.; Liu, P.; Chen, J. G. Tuning Selectivity of CO_2 Hydrogenation Reactions at the Metal/Oxide Interface. *J. Am. Chem. Soc.* **2017**, *139*, 9739–9754, DOI: 10.1021/jacs.7b05362.

(3) Behrens, M.; Studt, F.; Kasatkin, I.; Kühl, S.; Hävecker, M.; Abild-Pedersen, F.; Zander, S.; Girgsdies, F.; Kurr, P.; Kniep, B.-L.; Tovar, M.; Fischer, R. W.; Nørskov, J. K.; Schlögl, R. The Active Site of Methanol Synthesis over $Cu/ZnO/Al_2O_3$ Industrial Catalysts. *Science* **2012**, *336*, 893–897, DOI: 10.1126/science.1219831.

(4) Grabow, L. C.; Mavrikakis, M. Mechanism of methanol synthesis on Cu through CO_2 and CO hydrogenation. *ACS Catal.* **2011**, *1*, 365–384, DOI: 10.1021/cs200055d.

(5) Etim, U. J.; Song, Y.; Zhong, Z. Improving the Cu/ZnO-Based Catalysts for Carbon Dioxide Hydrogenation to Methanol, and the Use of Methanol As a Renewable Energy Storage Media. *Frontiers in Energy Research* **2020**, *8*, DOI: 10.3389/fenrg.2020.545431.

(6) Scotti, N.; Bossola, F.; Zaccheria, F.; Ravasio, N. Copper–Zirconia Catalysts: Powerful Multifunctional Catalytic Tools to Approach Sustainable Processes. *Catalysts* **2020**, *10*, 168, DOI: 10.3390/catal10020168.

(7) Arena, F.; Barbera, K.; Italiano, G.; Bonura, G.; Spadaro, L.; Frusteri, F. Synthesis, characterization and activity pattern of Cu–ZnO/ZrO_2 catalysts in the hydrogenation of carbon dioxide to methanol. *J. Catal.* **2007**, *249*, 185–194, DOI: 10.1016/j.jcat.2007.04.003.

(8) Arandia, A.; Yim, J.; Warraich, H.; Leppäkangas, E.; Bes, R.; Lempelto, A.; Gell, L.; Jiang, H.; Meinander, K.; Viinikainen, T.; Huotari, S.; Honkala, K.; Puurunen, R. L. Effect of atomic layer deposited zinc promoter on the activity of copper-on-zirconia catalysts in the hydrogenation of carbon dioxide to methanol. *Appl. Catal. B: Environ.* **2023**, *321*, 122046, DOI: 10.1016/j.apcatb.2022.122046.

(9) Wang, Y.; Kattel, S.; Gao, W.; Li, K.; Liu, P.; Chen, J. G.; Wang, H. Exploring the ternary interactions in Cu–ZnO–ZrO_2 catalysts for efficient CO_2 hydrogenation to methanol. *Nat. Comm.* **2019**, *10*, 1166, DOI: 10.1038/s41467-019-09072-6.

(10) Le Valant, A.; Comminges, C.; Tisseraud, C.; Canaff, C.; Pinard, L.; Pouilloux, Y. The Cu–ZnO synergy in methanol synthesis from CO2, Part 1: Origin of active site explained by experimental studies and a sphere contact quantification model on Cu + ZnO mechanical mixtures. *J. Catal.* **2015**, *324*, 41–49, DOI: 10.1016/j.jcat.2015.01.021.

(11) Vesborg, P. C.; Chorkendorff, I.; Knudsen, I.; Balmes, O.; Nerlov, J.; Molenbroek, A. M.; Clausen, B. S.; Helveg, S. Transient behavior of Cu/ZnO-based methanol synthesis catalysts. *J. Catal.* **2009**, *262*, 65–72, DOI: 10.1016/j.jcat.2008.11.028.

(12) Lunkenbein, T.; Schumann, J.; Behrens, M.; Schlögl, R.; Willinger, M. G. Formation of a ZnO Overlayer in Industrial Cu/ZnO/Al_2O_3 Catalysts Induced by Strong Metal-Support Interactions. *Angew. Chem. Int. Ed.* **2015**, *54*, 4544–4548, DOI: 10.1002/anie.201411581.

(13) Larmier, K.; Liao, W.-C. C.; Tada, S.; Lam, E.; Verel, R.; Bansode, A.; Urakawa, A.; Comas-Vives, A.; Copéret, C. CO_2-to-Methanol Hydrogenation on Zirconia-Supported Copper Nanoparticles: Reaction Intermediates and the Role of the Metal–Support Interface. *Angew. Chem. Int. Ed.* **2017**, *56*, 2318–2323, DOI: 10.1002/anie.201610166.

(14) Tang, Q.-L.; Hong, Q.-J.; Liu, Z.-P. CO_2 fixation into methanol at Cu/ZrO_2 interface from first principles kinetic Monte Carlo. *J. Catal.* **2009**, *263*, 114–122, DOI: 10.1016/j.jcat.2009.01.017.

(15) Kattel, S.; Ramírez, P. J.; Chen, J. G.; Rodriguez, J. A.; Liu, P. Active sites for CO_2 hydrogenation to methanol on Cu/ZnO catalysts. *Science* **2017**, *355*, 1296–1299, DOI: 10.1126/science.aal3573.

(16) Dharmalingam, B. C.; Koushik V, A.; Mureddu, M.; Atzori, L.; Lai, S.; Pettinau, A.; Kaisare, N. S.; Aghalayam, P.; Varghese, J. J. Unravelling the role of metal-metal oxide interfaces of $Cu/ZnO/ZrO_2/Al_2O_3$ catalyst for methanol synthesis from CO_2: Insights from experiments and DFT-based microkinetic modeling. *Appl. Catal. B: Environ.* **2023**, *332*, 122743, DOI: https://doi.org/10.1016/j.apcatb.2023.122743.

(17) Lempelto, A.; Gell, L.; Kiljunen, T.; Honkala, K. Exploring CO_2 hydrogenation to methanol at a CuZn-ZrO_2 interface via DFT calculations. *Catal. Sci. Technol.* **2023**, *13*, 4387–4399, DOI: 10.1039/d3cy00549f.

(18) Liu, X.; Luo, J.; Wang, H.; Huang, L.; Wang, S.; Li, S.; Sun, Z.; Sun, F.; Jiang, Z.; Wei, S.; Li, W.; Lu, J. In Situ Spectroscopic Characterization and Theoretical Calculations Identify Partially Reduced ZnO_{1-x}/Cu Interfaces for Methanol Synthesis from CO_2. *Angew. Chem. Int. Ed.* **2022**, *61*, e202202330, DOI: 10.1002/anie.202202330.

(19) Kauppinen, M.; Posada-Borbón, A.; Grönbeck, H. Methanol Synthesis Over PdIn, In_2O_3, and CuZn From First-Principles Microkinetics: Similarities and Differences. *J. Phys. Chem. C* **2022**, *126*, 15235–15246, DOI: 10.1021/acs.jpcc.2c05715.

(20) Dong, X.; Li, F.; Zhao, N.; Xiao, F.; Wang, J.; Tan, Y. CO_2 hydrogenation to methanol over $Cu/ZnO/ZrO_2$ catalysts prepared by precipitation-reduction method. *Appl. Catal. B: Environ.* **2016**, *191*, 8–17, DOI: https://doi.org/10.1016/j.apcatb.2016.03.014.

(21) Zhan, H.; Shi, X.; Tang, B.; Wang, G.; Ma, B.; Liu, W. The performance of Cu/Zn/Zr catalysts of different Zr/(Cu+Zn) ratio for CO_2 hydrogenation to methanol. *Catal. Commun.* **2021**, *149*, 106264, DOI: 10.1016/j.catcom.2020.106264.

(22) Huang, C.; Chen, S.; Fei, X.; Liu, D.; Zhang, Y. Catalytic Hydrogenation of CO_2 to Methanol: Study of Synergistic Effect on Adsorption Properties of CO_2 and H_2 in $CuO/ZnO/ZrO_2$ System. *Catalysts* **2015**, *5*, 1846–1861, DOI: 10.3390/catal5041846.

(23) Yang, M.; Yu, J.; Zimina, A.; Sarma, B. B.; Pandit, L.; Grunwaldt, J.; Zhang, L.; Xu, H.; Sun, J. Probing the Nature of Zinc in Copper-Zinc-Zirconium Catalysts by Operando Spectroscopies for CO_2 Hydrogenation to Methanol. *Angew. Chem. Int. Ed.* **2023**, *62*, DOI: 10.1002/anie.202216803.

(24) Zabilskiy, M.; Sushkevich, V. L.; Palagin, D.; Newton, M. A.; Krumeich, F.; van Bokhoven, J. A. The unique interplay between copper and zinc during catalytic carbon dioxide hydrogenation to methanol. *Nat. Commun.* **2020**, *11*, 2409, DOI: 10.1038/s41467-020-16342-1.

(25) Laudenschleger, D.; Ruland, H.; Muhler, M. Identifying the nature of the active sites in methanol synthesis over Cu/ZnO/Al2O3 catalysts. *Nat. Commun.* **2020**, *11*, DOI: 10.1038/s41467-020-17631-5.

(26) Beck, A.; Zabilskiy, M.; Newton, M. A.; Safonova, O.; Willinger, M. G.; van Bokhoven, J. A. Following the structure of copper-zinc-alumina across the pressure gap in carbon dioxide hydrogenation. *Nat. Catal.* **2021**, *4*, 488–497, DOI: 10.1038/s41929-021-00625-x.

(27) van Ommen, J. R.; Goulas, A.; Puurunen, R. L. Atomic Layer Deposition. In *Kirk-Othmer Encyclopedia of Chemical Technology*; Wiley, 2021; p 1–42, DOI: 10.1002/0471238961.koe00059.

(28) Zhang, B.; Qin, Y. Interface Tailoring of Heterogeneous Catalysts by Atomic Layer Deposition. *ACS Catal.* **2018**, *8*, 10064–10081, DOI: 10.1021/acscatal.8b02659.

(29) Kauppinen, M. M.; Melander, M. M.; Honkala, K. First-principles insight into CO hindered agglomeration of Rh and Pt single atoms on: M-ZrO_2. *Catal. Sci. Technol.* **2020**, *10*, 5847–5855, DOI: 10.1039/d0cy00413h.

(30) Di Liberto, G.; Pacchioni, G. Modeling Single-Atom Catalysis. *Adv. Mater.* **2023**, *35*, DOI: 10.1002/adma.202307150.

(31) Ouyang, R.; Liu, J.-X.; Li, W.-X. Atomistic Theory of Ostwald Ripening and Disintegration of Supported Metal Particles under Reaction Conditions. *J. Am. Chem. Soc.* **2013**, *135*, 1760–1771, DOI: 10.1021/ja3087054.

(32) Reichenbach, T.; Mondal, K.; Jäger, M.; Vent-Schmidt, T.; Himmel, D.; Dybbert, V.; Bruix, A.; Krossing, I.; Walter, M.; Moseler, M. Ab initio study of CO_2 hydrogenation mechanisms on inverse ZnO/Cu catalysts. *J. Catal.* **2018**, *360*, 168–174, DOI: 10.1016/j.jcat.2018.01.035.

(33) Reichenbach, T.; Walter, M.; Moseler, M.; Hammer, B.; Bruix, A. Effects of Gas-Phase Conditions and Particle Size on the Properties of Cu(111)-Supported Zn_yO_x Particles Revealed by Global Optimization and Ab Initio Thermodynamics. *J. Phys. Chem. C* **2019**, *123*, 30903–30916, DOI: 10.1021/acs.jpcc.9b07715.

(34) Mondal, K.; Megha,; Banerjee, A.; Fortunelli, A.; Walter, M.; Moseler, M. Ab Initio Modeling of the ZnO-Cu(111) Interface. *J. Phys. Chem. C* **2021**, *126*, 764–771, DOI: 10.1021/acs.jpcc.1c09170.

(35) Palomino, R. M.; Ramírez, P. J.; Liu, Z.; Hamlyn, R.; Waluyo, I.; Mahapatra, M.; Orozco, I.; Hunt, A.; Simonovis, J. P.; Senanayake, S. D.; Rodriguez, J. A. Hydrogenation of CO_2 on ZnO/Cu(100) and ZnO/Cu(111) Catalysts: Role of Copper Structure and Metal–Oxide Interface in Methanol Synthesis. *J. Phys. Chem. B* **2018**, *122*, 794–800, DOI: 10.1021/acs.jpcb.7b06901.

(36) Kuld, S.; Thorhauge, M.; Falsig, H.; Elkjaer, C. F.; Helveg, S.; Chorkendorff, I.; Sehested, J.; Elkjær, C. F.; Helveg, S.; Chorkendorff, I.; Sehested, J. Quantifying the promotion of Cu catalysts by ZnO for methanol synthesis. *Science* **2016**, *352*, 969–974, DOI: 10.1126/science.aaf0718.

(37) Fujitani, T.; Nakamura, J. *Catalysis Letters* **1998**, *56*, 119–124, DOI: 10.1023/a:1019000927366.

(38) Choi, Y.; Futagami, K.; Fujitani, T.; Nakamura, J. The role of ZnO in Cu/ZnO methanol synthesis catalysts — morphology effect or active site model? *Appl. Catal. A: Gen* **2001**, *208*, 163–167, DOI: 10.1016/s0926-860x(00)00712-2.

(39) Topsøe, N. Y.; Topsøe, H. On the nature of surface structural changes in Cu/ZnO methanol synthesis catalysts. *Top. Catal.* **1999**, *8*, 267–270, DOI: 10.1023/a:1019133832569.

(40) Grunwaldt, J. D.; Molenbroek, A. M.; Topsøe, N. Y.; Topsøe, H.; Clausen, B. S. In situ investigations of structural changes in Cu/ZnO catalysts. *J. Catal.* **2000**, *194*, 452–460, DOI: 10.1006/jcat.2000.2930.

(41) Kuld, S.; Conradsen, C.; Moses, P. G.; Chorkendorff, I.; Sehested, J. Quantification of Zinc Atoms in a Surface Alloy on Copper in an Industrial-Type Methanol Synthesis Catalyst. *Angew. Chem. Int. Ed.* **2014**, *53*, 5941–5945, DOI: 10.1002/anie.201311073.

(42) Amann, P.; Klötzer, B.; Degerman, D.; Köpfle, N.; Götsch, T.; Lömker, P.; Rameshan, C.; Ploner, K.; Bikaljevic, D.; Wang, H.-Y.; Soldemo, M.; Shipilin, M.; Goodwin, C. M.; Gladh, J.; Halldin Stenlid, J.; Börner, M.; Schlueter, C.; Nilsson, A. The state of zinc in methanol synthesis over a Zn/ZnO/Cu(211) model catalyst. *Science* **2022**, *376*, 603–608, DOI: 10.1126/science.abj7747.

(43) Enkovaara, J.; Rostgaard, C.; Mortensen, J. J.; Chen, J.; Dułak, M.; Ferrighi, L.; Gavnholt, J.; Glinsvad, C.; Haikola, V.; Hansen, H. A.; Kristoffersen, H. H.; Kuisma, M.; Larsen, A. H.; Lehtovaara, L.; Ljungberg, M.; Lopez-Acevedo, O.; Moses, P. G.; Ojanen, J.; Olsen, T.; Petzold, V.; Romero, N. A.; Stausholm-Møller, J.; Strange, M.; Tritsaris, G. A.; Vanin, M.; Walter, M.; Hammer, B.; Häkkinen, H.; Madsen, G. K. H.; Nieminen, R. M.; Nørskov, J. K.; Puska, M.; Rantala, T. T.; Schiøtz, J.; Thygesen, K. S.; Jacobsen, K. W. Electronic structure calculations with GPAW: a real-space

implementation of the projector augmented-wave method. *J. Phys. Cond. Mat.* **2010**, *22*, 253202, DOI: 10.1088/0953-8984/22/25/253202.

(44) Wellendorff, J.; Lundgaard, K. T.; Møgelhøj, A.; Petzold, V.; Landis, D. D.; Nørskov, J. K.; Bligaard, T.; Jacobsen, K. W. Density functionals for surface science: Exchange-correlation model development with Bayesian error estimation. *Phys. Rev. B* **2012**, *85*, 235149, DOI: 10.1103/PhysRevB.85.235149.

(45) Blöchl, P. E. Projector augmented-wave method. *Phys. Rev. B* **1994**, *50*, 17953–17979, DOI: 10.1103/PhysRevB.50.17953.

(46) Goedecker, S. Minima hopping: An efficient search method for the global minimum of the potential energy surface of complex molecular systems. *J. Chem. Phys.* **2004**, *120*, 9911–9917, DOI: 10.1063/1.1724816.

(47) Dudarev, S. L.; Botton, G. A.; Savrasov, S. Y.; Humphreys, C. J.; Sutton, A. P. Electron-energy-loss spectra and the structural stability of nickel oxide: An LSDA+U study. *Phys. Rev. B* **1998**, *57*, 1505–1509, DOI: 10.1103/PhysRevB.57.1505.

(48) Korpelin, V.; Melander, M. M.; Honkala, K. Reducing the Irreducible: Dispersed Metal Atoms Facilitate Reduction of Irreducible Oxides. *J. Phys. Chem. C* **2022**, *126*, 933–945, DOI: 10.1021/acs.jpcc.1c08979.

(49) Larsen, A. H.; Mortensen, J. J.; Blomqvist, J.; Castelli, I. E.; Christensen, R.; Dułak, M.; Friis, J.; Groves, M. N.; Hammer, B.; Hargus, C.; Hermes, E. D.; Jennings, P. C.; Jensen, P. B.; Kermode, J.; Kitchin, J. R.; Kolsbjerg, E. L.; Kubal, J.; Kaasbjerg, K.; Lysgaard, S.; Maronsson, J. B.; Maxson, T.; Olsen, T.; Pastewka, L.; Peterson, A.; Rostgaard, C.; Schiøtz, J.; Schütt, O.; Strange, M.; Thygesen, K. S.; Vegge, T.; Vilhelmsen, L.; Walter, M.; Zeng, Z.; Jacobsen, K. W. The atomic simulation environment—a Python library for working with atoms. *J. Phys. Condens. Mat.* **2017**, *29*, 273002.

(50) Bitzek, E.; Koskinen, P.; Gähler, F.; Moseler, M.; Gumbsch, P. Structural Relaxation Made Simple. *Phys. Rev. Lett.* **2006**, *97*, 170201, DOI: 10.1103/PhysRevLett.97.170201.

(51) Bader, R. F. W. *Atoms in Molecules: A Quantum Theory*; International series of monographs on chemistry; Oxford University Press: Oxford, 1990.

(52) Tang, W.; Sanville, E.; Henkelman, G. A grid-based Bader analysis algorithm without lattice bias. *J. Phys. Condens. Matter* **2009**, *21*, 084204, DOI: 10.1088/0953-8984/21/8/084204.

(53) Gattinoni, C.; Michaelides, A. Atomistic details of oxide surfaces and surface oxidation: the example of copper and its oxides. *Surf. Sci. Rep.* **2015**, *70*, 424–447, DOI: 10.1016/j.surfrep.2015.07.001.

(54) Crystallography Open Database. http://www.crystallography.net/cod/, (accessed 2023-05-11).

(55) Downs, R. T.; Hall-Wallace, M. The American Mineralogist Crystal Structure Database. *Am. Mineral.* **2003**, *88*, 247–250.

(56) Gražulis, S.; Chateigner, D.; Downs, R. T.; Yokochi, A. F. T.; Quirós, M.; Lutterotti, L.; Manakova, E.; Butkus, J.; Moeck, P.; Le Bail, A. Crystallography Open Database – an open-access collection of crystal structures. *J. Appl. Crystallogr.* **2009**, *42*, 726–729, DOI: 10.1107/S0021889809016690.

(57) Vaitkus, A.; Merkys, A.; Gražulis, S. Validation of the Crystallography Open Database using the Crystallographic Information Framework. *J. Appl. Crystallogr.* **2021**, *54*, 661–672, DOI: 10.1107/S1600576720016532.

(58) Sargeant, E.; Illas, F.; Rodríguez, P.; Calle-Vallejo, F. Importance of the gas-phase error correction for O2 when using DFT to model the oxygen reduc-

tion and evolution reactions. *J. Electroanal. Chem.* **2021**, *896*, 115178, DOI: 10.1016/j.jelechem.2021.115178.

(59) Almeida, M. O.; Kolb, M. J.; Lanza, M. R. V.; Illas, F.; Calle-Vallejo, F. Gas-Phase Errors Affect DFT-Based Electrocatalysis Models of Oxygen Reduction to Hydrogen Peroxide. *ChemElectroChem* **2022**, *9*, e202200210, DOI: 10.1002/celc.202200210.

(60) Montemore, M. M.; van Spronsen, M. A.; Madix, R. J.; Friend, C. M. O_2 Activation by Metal Surfaces: Implications for Bonding and Reactivity on Heterogeneous Catalysts. *Chem. Rev.* **2018**, *118*, 2816–2862, DOI: 10.1021/acs.chemrev.7b00217.

(61) Chase, M.; Davies, C.; Downey, J.; Frurip, D.; McDonald, R.; Syverud, A. *NIST JANAF thermochemical tables*; National Institute of Standards and Technology, Gaithersburg, 1986; DOI: 10.18434/T42S31.

(62) Reuter, K.; Scheffler, M. Oxide formation at the surface of late 4d transition metals: insights from first-principles atomistic thermodynamics. *Appl. Phys. A* **2004**, *78*, 793–798, DOI: 10.1007/s00339-003-2433-9.

(63) Thang, H. V.; Tosoni, S.; Fang, L.; Bruijnincx, P.; Pacchioni, G. Nature of Sintering-Resistant, Single-Atom Ru Species Dispersed on Zirconia-Based Catalysts: A DFT and FTIR Study of CO Adsorption. *ChemCatChem* **2018**, *10*, 2634–2645, DOI: https://doi.org/10.1002/cctc.201800246.

(64) Pacchioni, G. From CO_2 to Methanol on $Cu/ZnO/Al_2O_3$ Industrial Catalyst. What Do We Know about the Active Phase and the Reaction Mechanism? *ACS Catal.* **2024**, *14*, 2730–2745, DOI: 10.1021/acscatal.3c05669.

(65) Puigdollers, A. R.; Schlexer, P.; Tosoni, S.; Pacchioni, G. Increasing oxide reducibility: The role of metal/oxide interfaces in the formation of oxygen vacancies. *ACS Catal.* **2017**, *7*, 6493–6513, DOI: 10.1021/acscatal.7b01913.

(66) Bazhenov, A. S.; Kauppinen, M. M.; Honkala, K. DFT Prediction of Enhanced Reducibility of Monoclinic Zirconia upon Rhodium Deposition. *J. Phys. Chem. C* **2018**, *122*, 6774–6778, DOI: 10.1021/acs.jpcc.8b01046.

(67) Hinuma, Y.; Toyao, T.; Kamachi, T.; Maeno, Z.; Takakusagi, S.; Furukawa, S.; Takigawa, I.; Shimizu, K.-i. Density Functional Theory Calculations of Oxygen Vacancy Formation and Subsequent Molecular Adsorption on Oxide Surfaces. *J Phys. Chem. C* **2018**, *122*, 29435–29444, DOI: 10.1021/acs.jpcc.8b11279.

(68) Ozkan, D. M.; Uzun, A.; Caglayan, B. S.; Aksoylu, A. E. A DFT study on the role of oxygen vacancy on m-ZrO2 ($\bar{1}11$) in adsorption and dissociation of CO_2. *Surf. Sci.* **2023**, *736*, 122336, DOI: 10.1016/j.susc.2023.122336.

(69) Liu, J. Catalysis by Supported Single Metal Atoms. *ACS Catal.* **2017**, *7*, 34–59, DOI: 10.1021/acscatal.6b01534.

(70) Syzgantseva, O. A.; Calatayud, M.; Minot, C. Revealing the Surface Reactivity of Zirconia by Periodic DFT Calculations. *J. Phys. Chem. C* **2012**, *116*, 6636–6644, DOI: 10.1021/jp209898q.

(71) Zabilskiy, M.; Sushkevich, V. L.; Newton, M. A.; Van Bokhoven, J. A. Copper-Zinc Alloy-Free Synthesis of Methanol from Carbon Dioxide over Cu/ZnO/Faujasite. *ACS Catal.* **2020**, *10*, 14240–14244, DOI: 10.1021/acscatal.0c03661.

(72) Nakamura, J.; Choi, Y.; Fujitani, T. On the issue of the active site and the role of ZnO in Cu/ZnO methanol synthesis catalysts. *Top. Catal.* **2003**, *22*, 277–285, DOI: 1022-5528/03/0400{0277/0.

(73) Nakamura, J.; Fujitani, T.; Kuld, S.; Helveg, S.; Chorkendorff, I.; Sehested, J. Comment on "Active sites for CO_2 hydrogenation to methanol on Cu/ZnO catalysts. *Science* **2017**, *357*, eaan8074, DOI: 10.1126/science.aan8074.

(74) Beck, A.; Huang, X.; Artiglia, L.; Zabilskiy, M.; Wang, X. The dynamics of overlayer formation on catalyst nanoparticles and strong metal-support interaction. *Nat. Commun.* **2020**, *11*, 3220, DOI: 10.1038/s41467-020-17070-2.

(75) Wang, R.; Wang, H.; Weng, X.; Dai, J.; Gong, Z.; Zhao, C.; Lu, J.; Cui, Y.; Bao, X. Exploring the phase transformation in ZnO/Cu(111) model catalysts in CO_2 hydrogenation. *J. Energy Chem.* **2021**, *60*, 150–155, DOI: 10.1016/j.jechem.2020.12.023.

(76) Senanayake, S. D.; Ramírez, P. J.; Waluyo, I.; Kundu, S.; Mudiyanselage, K.; Liu, Z.; Liu, Z.; Axnanda, S.; Stacchiola, D. J.; Evans, J.; Rodriguez, J. A. Hydrogenation of CO_2 to Methanol on CeOx/Cu(111) and ZnO/Cu(111) Catalysts: Role of the Metal–Oxide Interface and Importance of Ce3+ Sites. *J. Phys. Chem. C* **2016**, *120*, 1778–1784, DOI: 10.1021/acs.jpcc.5b12012.

(77) Polierer, S.; Jelic, J.; Pitter, S.; Studt, F. On the Reactivity of the Cu/ZrO_2 System for the Hydrogenation of CO_2 to Methanol: A Density Functional Theory Study. *J. Phys. Chem. C* **2019**, *123*, 26904–26911, DOI: 10.1021/acs.jpcc.9b06500.

(78) Gell, L.; Lempelto, A.; Kiljunen, T.; Honkala, K. Influence of a Cu–zirconia interface structure on CO_2 adsorption and activation. *J. Chem. Phys.* **2021**, *154*, 214707, DOI: 10.1063/5.0049293.

(79) Dietze, E. M.; Abild-Pedersen, F.; Plessow, P. N. Comparison of Sintering by Particle Migration and Ripening through First-Principles-Based Simulations. *J. Phys. Chem. C* **2018**, *122*, 26563–26569, DOI: 10.1021/acs.jpcc.8b09303.

(80) Hu, S.; Li, W.-X. Sabatier principle of metal-support interaction for design of ultrastable metal nanocatalysts. *Science* **2021**, *374*, 1360–1365, DOI: 10.1126/science.abi9828.

(81) Sehested, J. Industrial and scientific directions of methanol catalyst development. *J. Catal.* **2019**, *371*, 368–375, DOI: 10.1016/j.jcat.2019.02.002.

(82) Nakamura, J.; Nakamura, I.; Uchijima, T.; Watanabe, T.; Fujitani, T. Model studies of methanol synthesis on copper catalysts. *Stud. Surf. Sci. Catal.* **1996**, *101 B*, 1389–1399, DOI: 10.1016/s0167-2991(96)80351-x.

(83) Zander, S.; Kunkes, E. L.; Schuster, M. E.; Schumann, J.; Weinberg, G.; Teschner, D.; Jacobsen, N.; Schlögl, R.; Behrens, M. The role of the oxide component in the development of copper composite catalysts for methanol synthesis. *Angew. Chem. Int. Ed.* **2013**, *52*, 6536–6540, DOI: 10.1002/anie.201301419.

(84) Kattel, S.; Ramírez, P. J.; Chen, J. G.; Rodriguez, J. A.; Liu, P. Response to Comment on "Active sites for CO_2 hydrogenation to methanol on Cu/ZnO catalysts. *Science* **2017**, *357*, eaan8210, DOI: 10.1126/science.aan8210.

(85) Koitaya, T.; Yamamoto, K.; Uruga, T.; Yokoyama, T. Operando Characterization of Copper–Zinc–Alumina Catalyst for Methanol Synthesis from Carbon Dioxide and Hydrogen by Ambient-Pressure Hard X-ray Photoelectron Spectroscopy. *J. Phys. Chem. C* **2023**, *127*, 13044–13054, DOI: 10.1021/acs.jpcc.3c02785.

(86) Agrell, J.; Birgersson, H.; Boutonnet, M.; Melián-Cabrera, I.; Navarro, R.; Fierro, J. Production of hydrogen from methanol over Cu/ZnO catalysts promoted by ZrO_2 and Al_2O_3. *J. Catal.* **2003**, *219*, 389–403, DOI: https://doi.org/10.1016/S0021-9517(03)00221-5.

(87) Studt, F.; Behrens, M.; Kunkes, E. L.; Thomas, N.; Zander, S.; Tarasov, A.; Schumann, J.; Frei, E.; Varley, J. B.; Abild-Pedersen, F.; Nørskov, J. K.; Schlögl, R. The Mechanism of CO and CO_2 Hydrogenation to Methanol over Cu-Based Catalysts. *ChemCatChem* **2015**, *7*, 1105–1111, DOI: 10.1002/cctc.201500123.

(88) Kopač, D.; Likozar, B.; Huš, M. Catalysis of material surface defects: Multiscale modeling of methanol synthesis by CO_2 reduction on copper. *Appl. Surf. Sci.* **2019**, *497*, 143783, DOI: 10.1016/j.apsusc.2019.143783.

(89) Cao, A.; Wang, Z.; Li, H.; Elnabawy, A. O.; Nørskov, J. K. New insights on CO and CO_2 hydrogenation for methanol synthesis: The key role of adsorbate-adsorbate interactions on Cu and the highly active MgO-Cu interface. *J. Catal.* **2021**, *400*, 325–331, DOI: https://doi.org/10.1016/j.jcat.2021.06.020.

TOC Graphic